

A Synchronization Method for Synchronous CDMA Broadband Communication Systems with GEO Satellites

Takuya SAKAMOTO^{†a)}, Student Member, Daisuke UMEHARA[†], Member, Yoshiteru MORIHIRO[‡], Fellow, and Makoto KAWAI^{††}, Member

SUMMARY High speed core networks with optical fibers have spread widely, but it is still difficult to access the core networks from many rural areas. Synchronous CDMA systems with GEO satellite links are attractive to solve this problem, since they have wide service areas and are suitable for packet-based networks due to their statistically multiplexing effects. Additionally, the synchronous CDMA systems have more effective frequency utilization and power efficiency than asynchronous ones. In the synchronous CDMA systems, transmitted signals from fixed earth stations are required to achieve synchronization with each other. The broadband systems require extremely precise timing control as their bit rates increase. In this paper, we propose a synchronization method for a synchronous CDMA communication system using a GEO satellite and verify the feasibility of Gigachip rate synchronous CDMA systems.

key words: synchronous CDMA, GEO satellite, synchronization method, Kalman filter

1. Introduction

Recently, packet-based data communications for multimedia services attract a great deal of attention. High speed core networks for data communications have spread widely, but it is still difficult to access the core networks from rural areas. GEO (Geosynchronous Orbit) satellite communication systems provide a solution to connect rural areas with core networks due to their wide service areas. A multiple access technique is indispensable for a communication system including multiple FESs (Fixed Earth Stations). CDMA (Code Division Multiple Access) systems are suitable for packet-based networks because they have statistically multiplexing effects. Packets are transmitted intermittently, which is different from the case of circuit switching. The instantaneous number of users can be reduced by using packet switching. By assigning a code to each FES preliminarily, this effect can be effectively utilized as compared to FDMA or TDMA which require over-head time for on-demanding. However, asynchronous CDMA systems have lower frequency utilization and power efficiency than conventional multiple access techniques like FDMA or TDMA. In order to overcome this drawback, we try to apply synchronous CDMA to GEO satellite communication systems. The synchronous CDMA system can utilize pseudo-noise

codes which have less cross correlation with each other under the perfect synchronization among codes. However, in the synchronous CDMA systems, a transmitted signal from each FES is required to achieve synchronization with other FESs. Additionally, broadband systems require extremely precise timing control as their bit rates increase.

There are several works examining synchronization accuracy of synchronous systems [1]–[4]. They utilize fixed filters for synchronization. The accuracy of the fixed filters are enough if their targets are narrow-band systems. However, the synchronization accuracy is not sufficient for the broadband systems which this paper aims at. Kalman filter is known as the optimum filter on the conditions as the linearity of a system equation, the whiteness of noise, a Gaussian probability density function (PDF) of the noise, and a quadratic criteria for estimation. However, Kalman filter has not been considered to apply to a synchronization method for CDMA satellite communications. Additionally, conventional studies deal only with simple waveform like a step function or a ramp function as delay scintillation, which is not enough to evaluate the synchronization accuracy in a real system quantitatively.

In this paper, we consider to apply Kalman filter to a synchronization method and describe the problems to use conventional ordinary Kalman filter. We propose a new method to solve the problems. Next, we investigate and evaluate the synchronization accuracy with more realistic signals than the conventional simple ones. We clarify that a fixed filter and conventional ordinary Kalman filter are not enough to obtain the accuracy required to implement Gigachip rate. We also clarify that the proposed method can improve the performance and make the synchronous Gigachip rate CDMA feasible for the broadband communication systems with a GEO satellite [5].

2. System and Delay Scintillation Models

2.1 System Model

In this section, we describe our system model. Figure 1 shows an example of communication links of the assumed system. Each FES in rural areas can access core network via a satellite link as in this figure. A multiplexing technique is required for this system because one satellite is utilized by all the FESs in common. Figure 2 shows the system model assumed in this paper. We assume a GEO satellite, an NCS

Manuscript received November 22, 2003.

Manuscript revised March 8, 2004.

[†]The authors are with the Department of Communications and Computer Engineering, Graduate School of Informatics, Kyoto University, Kyoto-shi, 606-8501 Japan.

^{††}The author is with the Faculty of Science and Engineering, Ritsumeikan University, Kusatsu-shi, 525-8577 Japan.

a) E-mail: t-sakamo@aso.cce.i.kyoto-u.ac.jp

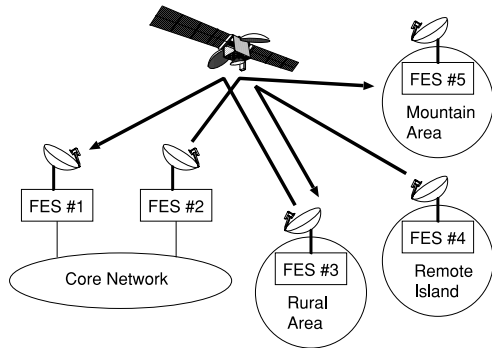


Fig. 1 Communication links between the core network and rural areas.

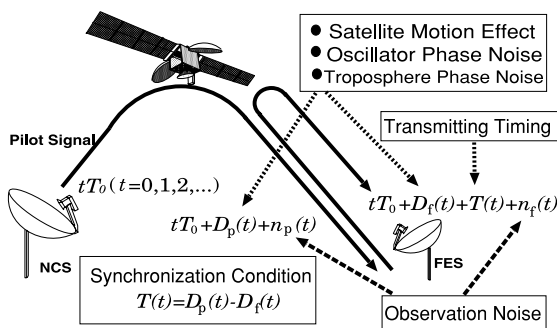


Fig. 2 System model of a synchronous CDMA communication system with a GEO satellite.

(Network Control Station) and multiple FESs in the system. We assume a direct sequence synchronous CDMA system. The synchronous CDMA system can utilize codes which have less cross correlation. Therefore, the NCS transmits pilot signals at T_0 intervals in order to synchronize FESs with each other. We assume that the GEO satellite has a bent-pipe function. The number of satellite beams is one and each FES receives its own returned signal and the pilot signal transmitted from the NCS.

One of spreading sequences is assigned to the NCS and the others are assigned to FESs. For example, we can assume the synchronous CDMA system with data rate of 3.6 Mbps, 256 FESs and processing gain of 24 dB. Each FES's data is modulated with QPSK and spread with a spreading code. As for error correction codes, we utilize a Reed-Solomon code (204,188) as an outer code, a convolutional code ($K = 7$, coding rate of 1/2) as an inner code. This system has the chip rate of about 1Gchip/sec. When we use Ka band, this system is feasible in regard to bandwidth and high-power amplifier availability. The bandwidth of 1 GHz can be used in Ka-band in which the bandwidth of 3.5 GHz is allocated. Regarding high power amplifier, TWTAs (Traveling Wave Tube Amplifiers) are utilized for Ka-band communications. The TWTAs have a wide bandwidth, which can be used for broadband communications. Recently, multi-port amplifiers have been developed for high-power transmitting. For example, an 8-port amplifier is planned to be implemented in WINDS (Wide-

Table 1 An example of parameters of a FES.

Antenna	Offset Parabola (ϕ 80cm)
Max. Trans. Power	8 W
Noise Temperature	200 K
Modulation	QPSK and Spectrum Spreading
Outer Code	Reed-Solomon Code (204,188)
Inner Code	Convolutional Code/Viterbi Decoding
	$K = 7$ (1/2)
Data Rate	3.6 Mbps

Table 2 An example of communication link (3.6 Mbps).

FES EIRP	52.5 dBW
Up Loss	-214.0 dB
Satellite G/T	14.2 dB/K
Satellite EIRP	43.0 dBW
Down Loss	-210.0 dB
FES G/T	15.5 dB/K
Equiv. Noise Bandwidth	-65.9 dBHz
Total C/N	9.8 dB
E_b/N_0	10.2 dB

Table 3 Parameters in this paper.

Satellite location	East longitude 132°
Eccentricity	0.0005
Orbital inclination angle	0.05°
NCS location	The center of Tokyo
Update period T_0	1sec

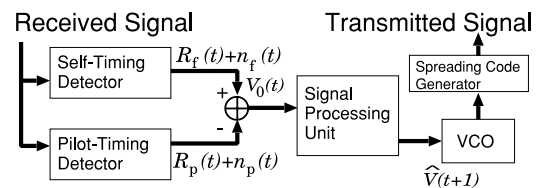


Fig. 3 Block diagram of a receiver and a transmitter.

band InterNetworking engineering test and Demonstration Satellite) [6]. This amplifier has maximum output power over 280 W (EIRP is more than 67 dBW) and bandwidth of 1.1 GHz. As for FES amplifiers, we can utilize a high-power solid state amplifier [7]. This amplifier has a bandwidth from 25 GHz to 31 GHz and output power of 25 W. Tables 1 and 2 show examples of FES parameters and a communication link design, respectively. This design is based on the study of the reference paper [8].

The reference paper [1] shows that synchronous CDMA systems are able to have good performance only if the RMS (Root Mean Square) of synchronization errors are within 0.3 of the chip duration. It means that the system with the chip rate of 1 Gchip/sec requires the synchronization accuracy of 0.3 nsec. Table 3 shows the assumed parameters for the system considered in this paper.

2.2 Synchronization Principle

Figure 3 illustrates a block diagram of a receiver and a transmitter in the FESs. Each FES measures the receiving time of the pilot signal and its own returned signal at intervals of

T_0 using the self timing detector and pilot timing detector, where T_0 is an update period shown in Table 3. The suffixes p and f indicate the NCS and FES, respectively. We assume that the NCS has a base clock $T_{b,p}(t) = tT_0 + \tilde{T}_{b,p}(t)$ and the FES has a base clock $T_{b,f}(t) = tT_0 + \tilde{T}_{b,f}(t)$ for $t = 0, 1, \dots$ where $\tilde{T}_{b,p}(t)$ and $\tilde{T}_{b,f}(t)$ are random signals caused by oscillator phase noise. The transmitting time of the FES's signal $T_f(t)$ is expressed as

$$T_f(t) = T_{b,f}(t) + T(t) + \tilde{T}(t), \quad (1)$$

where $T(t)$ is a timing offset for synchronization and $\tilde{T}(t)$ is a random signal caused by oscillator phase noise. The time receiving the FES's returned signal $R_f(t)$ is expressed as

$$R_f(t) = T_{b,f}(t) + T(t) + \tilde{T}(t) + D_f^*(t), \quad (2)$$

where $D_f^*(t)$ is delay time of the returned signal. The DC component of $D_f^*(t)$ is turn around time, which does not relate to synchronization accuracy. The other factors of $D_f^*(t)$ are caused mainly by troposphere phase scintillation and satellite motion effect. Here, we can neglect the effect of ionospheric irregularities because the frequency band is Ka-band which has little interaction with ionosphere. The pilot signal transmitting time $T_p(t)$ is expressed as

$$T_p(t) = T_{b,p}(t) = tT_0 + \tilde{T}_{b,p}(t), \quad (3)$$

which means that the pilot signal is transmitted periodically. The time receiving pilot signal $R_p(t)$ is expressed as

$$R_p(t) = T_{b,p}(t) + D_p^*(t), \quad (4)$$

where $D_p^*(t)$ is delay time of the pilot signal.

Synchronization error $e(t)$ is expressed as $e(t) = R_f(t) - R_p(t)$. It is required to satisfy $e(t) = 0$ to achieve complete synchronization. If $e(t) = 0$ for all FESs, then we can achieve the perfect synchronization among codes. $e(t)$ can be also expressed as

$$e(t) = T(t) - V(t), \quad (5)$$

where

$$V(t) = D_p^*(t) - D_f^*(t) + \tilde{T}_{b,p}(t) - \tilde{T}_{b,f}(t) - \tilde{T}(t). \quad (6)$$

In order to reduce the RMS of $e(t)$, we should estimate $V(t)$ and set $T(t) = \hat{V}(t)$, where $\hat{V}(t)$ is estimated $V(t)$. We define $V_0(t)$ as the observed $V(t)$. $V_0(t)$ contains the observation noise denoted by $n_f(t)$ for FESs and $n_p(t)$ for NCS as in Fig. 3. These observation noises mean the timing error caused by additive noise in the received signal. The signal processing unit in Fig. 3 calculates $\hat{V}(t+1)$ by utilizing $V_0(i)$ ($i = 0, 1, \dots, t$). $\hat{V}(t+1)$ is input into VCO (Voltage Controlled Oscillator) and the timing offset $T(t+1) = \hat{V}(t+1)$ is updated.

2.3 Delay Scintillation Model

We investigate propagation characteristics in order to eval-

uate the synchronization accuracy. The observed delay difference $V_0(t)$ equals to the sum of the following four factors and a DC component.

1. Satellite motion effect $s_{\text{sat}}(t)$
2. Observation noises $n(t) = n_f(t) - n_p(t)$
3. Oscillator phase noise $O(t) = \tilde{T}(t) + \tilde{T}_{b,f}(t) - \tilde{T}_{b,p}(t)$
4. Troposphere phase scintillation $T_t(t)$

The satellite motion effect and the troposphere phase scintillation give the equation

$$D_p^*(t) - D_f^*(t) = s_{\text{sat}}(t) + T_t(t). \quad (7)$$

We explain the four factors of delay scintillation in detail in the following.

First, we investigate the satellite motion effect in terms of delay scintillation. We detail the satellite motion effect and its amplitude in Appendix. The delay scintillation caused by the motion of a satellite is approximately expressed as

$$s_{\text{sat}}(t) \approx A_{\text{sat}} \sin(\omega T_0 t + \phi), \quad (8)$$

where $\omega = 2\pi/(24 \times 60 \times 60)$ rad/sec and A_{sat} depends on the location of FES. The amplitude of A_{sat} is shown in Fig. 4. As we see in Fig. 4, the place with the maximum A_{sat} is Hateruma of Okinawa in Japan. We can calculate the maximum A_{sat} which is 3618 nsec at most in Japan. We adopt this value because our purpose is to evaluate synchronization accuracy at the worst case. If $s_{\text{sat}}(t)$ is a perfect sinusoid, we can exactly estimate the effects of $s_{\text{sat}}(t)$. However, $s_{\text{sat}}(t)$ is not a perfect sinusoid but modulated by a random factor. We should estimate $s_{\text{sat}}(t)$ each T_0 interval.

The effects of $O(t)$ and $T_t(t)$ are expressed as stochastic processes whose power spectra are known. We utilize the measured spectra of Italsat beacon signal as $O(t)$ and $T_t(t)$. The power spectra of $O(t)$ and $T_t(t)$ are expressed as $Af^{-\alpha}$, where f is the frequency.

It is known that $\alpha = 3$ and $A = 1/(40 \times 10^9 \pi)$ sec for

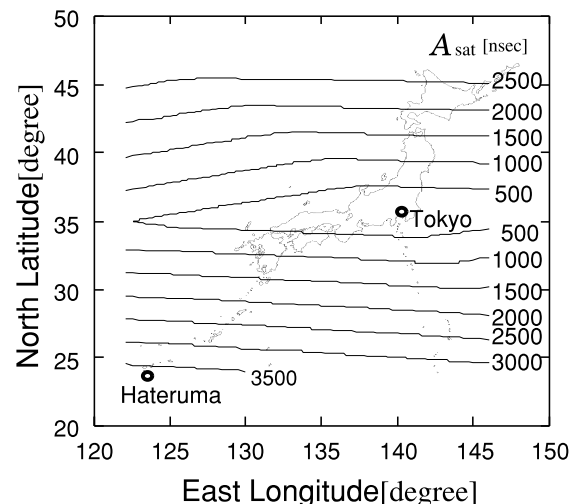


Fig. 4 Amplitude of satellite motion effect in Japan [nsec].

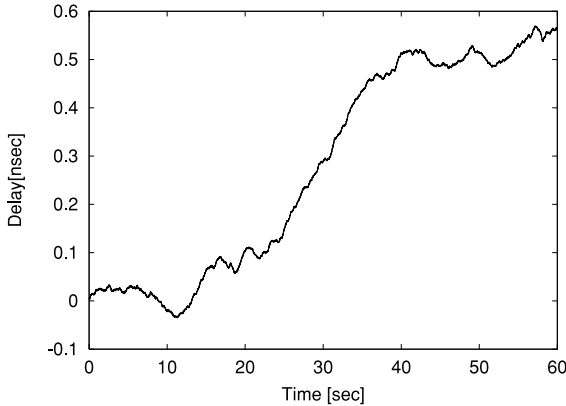


Fig. 5 An example of delay scintillation $V(t)$.

$O(t)$ [9]. For our system model, we should adopt $3Af^{-\alpha}$ because $O(t)$ is the sum of three oscillator phase noises as $O(t) = \tilde{T}(t) + \tilde{T}_{b,f}(t) - \tilde{T}_{b,p}(t)$.

The theory of isotropic turbulence gives $T_t(t)$ for 30 GHz as $\alpha = 8/3$ and $A = 1.941 \times (4/3)^2 \times \nu^{5/3} C_n^2 L$, where ν is the cross-path wind component and $C_n^2 L$ is path turbulence index. We set $\nu = 8$ m/sec for the cross-path wind component. It is known that $3 \times 10^{-11} \leq C_n^2 L \leq 6 \times 10^{-8} \text{ m}^{1/3}$ is satisfied [10], [11]. We adopt $C_n^2 L = 6 \times 10^{-8} \text{ m}^{1/3}$ because we evaluate the worst case. We set $4Af h^{-\alpha}$ as the spectrum because $D_f^*(t)$ and $D_p^*(t)$ contain a round-trip path of troposphere, respectively. As for $n(t)$, we assume that it can be regarded as white Gaussian noise whose standard deviation is 0.5 nsec. This assumption corresponds to S/N = 9 dB after despreading, which is valid for evaluating the worst case of real systems [12].

Figure 5 shows an example of $V(t)$ based on the above considerations. Here we assume that $A_{\text{sat}} = 100$ nsec and $\phi = 0$ rad. Other parameters correspond to the worst case described above. We see that $V(t)$ has a large trend component, which changes slowly compared to the observation time. The large trend component is generated by the satellite motion effect.

3. Synchronization Methods

3.1 Fixed Filter

Conventional studies [2] dealt with a fixed filter for synchronization such as

$$\Lambda(z) = \frac{1}{4} \cdot \frac{2z^{-1} - z^{-2}}{1 - 2z^{-1} + z^{-2}}. \quad (9)$$

The fixed filter method estimates $V(t)$ by calculating $\hat{V}(t+1) = \hat{V}(t) - \gamma(t)$ and $\Gamma(z) = \Lambda(z)E(z)$, where $\Gamma(z)$ and $E(z)$ are the z-transform of $\gamma(t)$ and $e(t)$, respectively.

We consider on filters used for CDMA synchronization. First, we apply the fixed filter to $V(t)$ shown as an example of realistic signal of $V(t)$ in the previous section and evaluate the synchronization accuracy. The simulation model for the evaluation is described in the next section. We

have confirmed the synchronization accuracy of the fixed filter is 0.470 nsec, which is insufficient for the assumed system. The PDF of the synchronization error for the fixed filter is shown in Fig. 11. Therefore, we investigate to apply Kalman filter to synchronization.

3.2 Kalman Filter

Kalman filter is known as the optimum filter only if the system parameters are completely known. Kalman filter requires the system parameters which describe the characteristic of $V(t)$. We assume that $V(t)$ is approximately generated by the linear system expressed as

$$\begin{aligned} \mathbf{x}_{t+1} &= F\mathbf{x}_t + G\mathbf{w}_t, \\ V(t) &= H\mathbf{x}_t + \mathbf{v}_t, \end{aligned} \quad (10)$$

where \mathbf{x}_t is an L -dimensional state vector, \mathbf{w}_t is a 1-dimensional plant noise vector, \mathbf{v}_t is a 1-dimensional observation noise vector, F is an $L \times L$ state transition matrix, G is an $L \times 1$ driving matrix, and H is a $1 \times L$ observation matrix. Under the above-mentioned assumption, Kalman filter is able to estimate $V(t)$ using $V_0(i)$ ($i = 0, 1, \dots, t-1$) [13].

In order to use Kalman filter, we should determine the system parameters in Eq. (10). In a real system, the system parameters should be updated periodically because the characteristic of $V(t)$ is changeable. We use auto regressive (AR) equation to determine the system parameters in Eq. (10). First, let us assume that $V(t)$ is represented as the output of the L -th order of AR-equation. The L -th order of AR equation is expressed as

$$V(t) + \sum_{m=1}^L a_m V(t-m) = W_t, \quad (11)$$

where W_t is white Gaussian noise and a_m is the m -th coefficient of AR-equation. We can determine a_m and the RMS of W_t using the maximum likelihood criterion. If the number of data is larger enough compared to L , the maximum likelihood criterion approximately becomes equal to the least square problem which is expressed as

$$\text{minimize} \sum_t \left\{ V(t) + \sum_{m=1}^L a_m V(t-m) \right\}^2. \quad (12)$$

If the parameters in AR equation is determined, it can be translated into the matrices F, G, H in Eq. (10) as

$$F = \begin{bmatrix} -a_1 & -a_2 & \cdots & -a_{L-1} & -a_L \\ 1 & & & \mathbf{O} & 0 \\ & 1 & & & 0 \\ \mathbf{O} & & \ddots & & \vdots \\ & & & 1 & 0 \end{bmatrix}, \quad (13)$$

$$G = \begin{bmatrix} 1 \\ 0 \\ \vdots \\ 0 \end{bmatrix}, \quad H = \begin{bmatrix} 1 \\ 0 \\ \vdots \\ 0 \end{bmatrix}^T. \quad (14)$$

In a real system, $V(t)$ should be estimated in real-time. If we adopt large dimension L for Kalman filter, it is difficult to satisfy the condition of calculation time because calculation time of Kalman filter significantly increases for large L . Therefore, we should restrict the dimension of Kalman filter. We call Kalman filter with limited dimension DLKF (Dimension Limited Kalman Filter).

We have to determine the dimension of DLKF before determining the system parameters. We calculate AIC (Akaike Information Criterion) in order to determine L because AIC is known as a validation criterion for a model to express a signal [14]. AIC is given as

$$AIC = N \log \left\{ 2\pi\sigma_L^2 \left(1 - \frac{L}{N} \right) \right\} + N + 2(L + 1), \quad (15)$$

where N is the number of data and σ_L^2 is the estimated power of the white Gaussian noise for the L -th order of AR equation. We utilize the Levenberg-Marquardt method to solve the optimization problem in Eq. (12) in order to calculate AIC [15]. Levenberg-Marquardt method is a well-known algorithm for nonlinear optimization. Figure 6 shows the relationship between L and AIC for the numerically generated data $V(t)$ for $A_{\text{sat}} = 0$ nsec and $N = 10000$. $A_{\text{sat}} = 0$ nsec means the situation where $s_{\text{sat}}(t)$ is negligible. $N = 10000$ means that the duration of the data is 10000sec. In expressing a random signal using an AR-equation, an extremely low frequency signal like $s_{\text{sat}}(t)$ degrades the accuracy. It is not valid to determine a model using AIC with the degraded estimation in the AR-equation. Therefore, we utilize the condition $A_{\text{sat}} = 0$ nsec. Estimating a_1, a_2, \dots, a_L using Eq. (12) requires the condition that N is sufficiently large for L as described above. We adopt $N = 10000$, which is sufficiently large compared to the acceptable maximum L . We see that the AIC changes comparatively little for $L \geq 3$. We adopt $L = 3$ because smaller L is required. Next, we solve the optimization problem in Eq. (12) and obtain the system parameters which generates $V(t)$. The determined system parameters are $a_1 = -1.644964, a_2 = 0.487694$ and $a_3 = 0.156907$ by using the Levenberg-Marquardt method. We utilize these system parameters for DLKF.

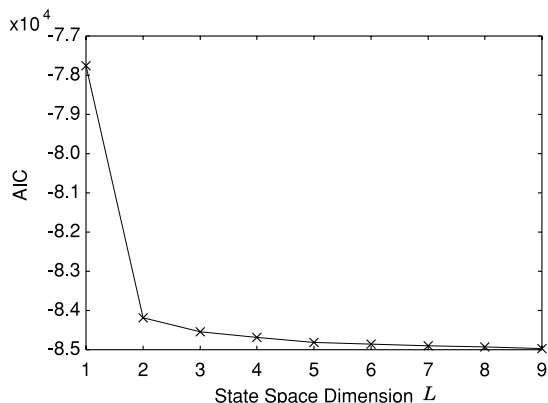


Fig. 6 Relationship between AIC and dimension.

3.3 Modified Kalman Filter

Here, we discuss the validity of the assumed linear system for DLKF. The power spectrum of the signal generated by an AR-equation is called an AR-spectrum. The AR-spectrum for the L -th order of AR equation is given by

$$S(\omega) = \frac{\sigma^2}{\left| 1 + \sum_{m=1}^L a_m e^{-jmT_0\omega} \right|^2}, \quad (16)$$

where σ is the standard deviation of W_t . It is known that accurate synchronization requires that $S(\omega)$ is similar to the power spectrum of $V(t)$. However, the width of this spectrum depends on the dimension L . In general, small L makes the spectrum wide, which is a serious problem.

Figure 7 shows an example of the power spectrum of $V(t)$. We assume that $s_{\text{sat}}(t)$ is a randomly modulated sinusoid whose relative bandwidth is 2.5%. As for other random signals, we adopt parameters for the worst case described in Section 2.3. The solid line in the figure shows an example of the power spectrum of $V(t)$, and the broken line shows an example of the 3rd order of AR-spectrum for $a_1 = -1.644964, a_2 = 0.487694$ and $a_3 = 0.156907$. We should note that $s_{\text{sat}}(t)$ is not a simple sinusoid but a modulated one. Here, we assume $s_{\text{sat}}(t)$ is a randomly modulated sinusoid. The gentle slope in the figure corresponds to the troposphere phase scintillation $T_t(t)$ and oscillator phase noise $O(t)$. The steep peak in the figure is caused by $s_{\text{sat}}(t)$. It is impossible to express $s_{\text{sat}}(t)$ with $L = 3$ because large L is required to express $s_{\text{sat}}(t)$. For example, expressing a periodic function with a 24-hours period requires at least $L = 60 \times 60 \times 24$ because we have set the update period $T_0 = 1$ sec.

Since the whole characteristics of $V(t)$ cannot be expressed using a linear system with small L we propose a new method to solve this problem. We can deal with $s_{\text{sat}}(t)$ as a linear function in a short duration. We utilize this characteristic of $s_{\text{sat}}(t)$. The proposed algorithm deals with $s_{\text{sat}}(t)$ and others separately. We call the new method KFMT (Kalman Filter Method for signals with Trend components). Note

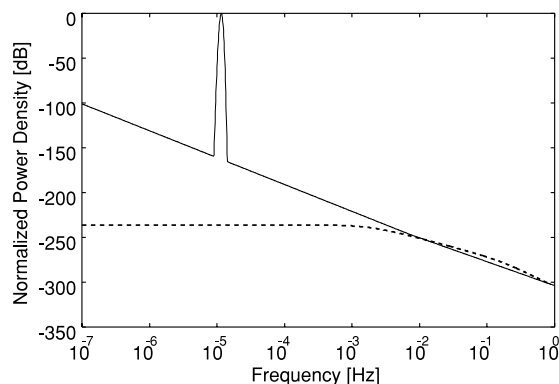


Fig. 7 An example of power spectrum of $V(t)$.

that KFMT method is an extended DLKF method by compensating for a trend component using a straight line. The algorithm of KFMT is as follows.

1. The regression line $r_t(i)$ ($i = 0, \dots, t$) is calculated using $V(t-M), \dots, V(t-1)$.
2. The temporal estimated value $\hat{V}_{tmp}(t)$ is obtained by applying DLKF method to $V(t-1) - r_t(t-1)$.
3. The final estimated value $\hat{V}(t)$ is obtained as $\hat{V}(t) = \hat{V}_{tmp}(t) + r_t(t)$.

The flow diagram of KFMT method is shown in Fig. 8. Dealing with $s_{sat}(t)$ as a linear function is approximately equivalent to applying a low frequency suppression filter in the frequency domain. We can suppress $s_{sat}(t)$ by utilizing this nature. Besides we can suppress a high frequency signal with the Kalman filter. The algorithm shown in Fig. 8 suppresses a low frequency signal using the last M data by eliminating the estimated linear function, which leads to making the output signal close to the estimated AR-spectrum. Next, this algorithm estimates the high frequency signal on the next step by applying DLKF which assumes the estimated AR-spectrum.

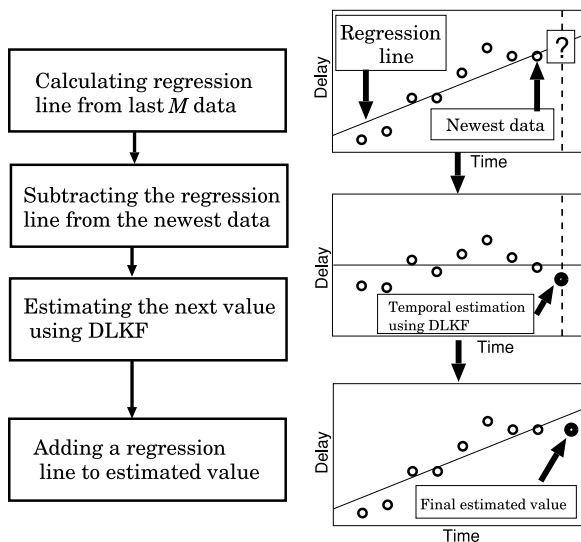


Fig. 8 Flow diagram of KFMT method.

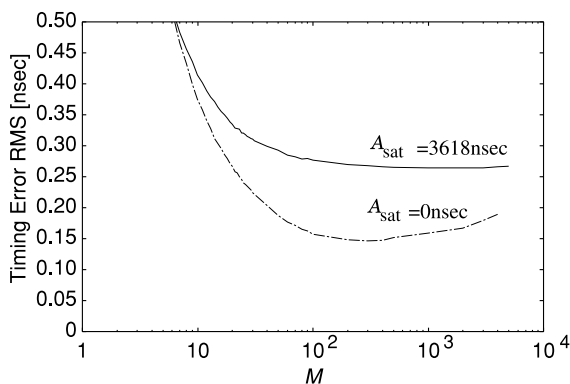


Fig. 9 Relationship between synchronization accuracy and M .

Next, we must select an appropriate parameter M in KFMT. If M is small, the estimation of a regression line becomes unstable. On the other hand, if M is large, $s_{sat}(t)$ cannot be approximated as a linear function. The relationship between synchronization accuracy and M is shown in Fig. 9. We see the curve is downwards convex and $M \approx 100 \sim 1000$ gives the acceptable synchronization error in the figure. We select $M = 100$ based on the condition above.

4. Synchronization Accuracy Evaluation

4.1 Simulation Model

We have proposed DLKF method and KFMT method in the previous section. Both of them have approximately the same computational complexity. In this section, we investigate the synchronization accuracy for the synchronization methods DLKF and KFMT using realistic signals of $V(t)$. Figure 10 shows the numerical simulation model used in this paper. We set each filter to “Estimation Filter” block and obtain synchronization error $e(t)$ for each filter.

4.2 Calculation Results

Here, we calculate the distribution of the estimation error $e(t)$, on the condition of $A_{sat} = 3618$ nsec and $\sigma_v = 0.5$ nsec. We calculate the PDF in order to evaluate the accuracy of synchronization methods. We apply the methods to the data for 10000sec when $s_{sat}(t)$ has the steepest inclination. The PDF of a synchronization error is shown in Fig. 11. The synchronization accuracy for the fixed filter is 0.470 nsec. The synchronization accuracy for DLKF is 0.702 nsec, which is larger than the aimed accuracy of 0.3 nsec. Its poor perfor-

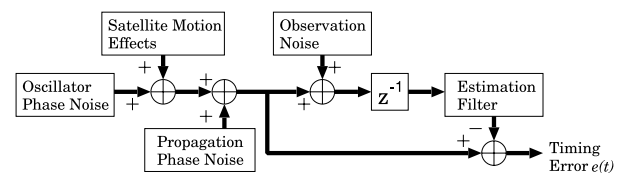


Fig. 10 Simulation model.

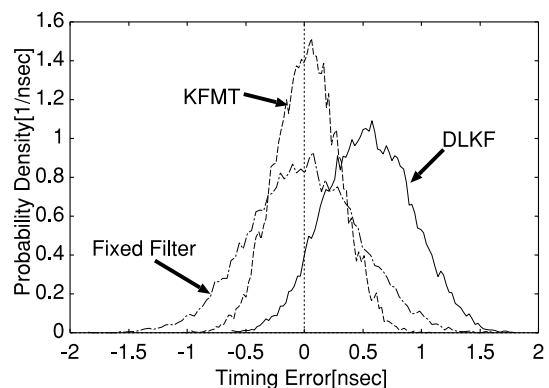


Fig. 11 PDFs of synchronization errors.

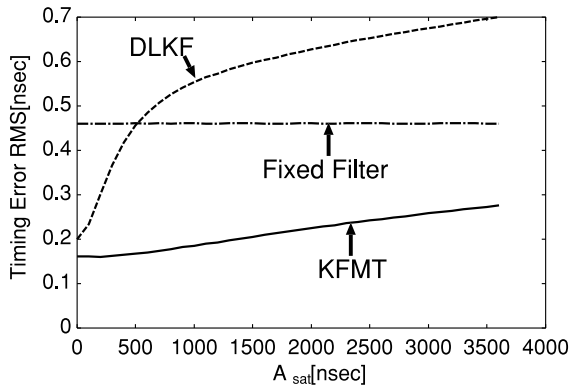


Fig. 12 Relationship between synchronization accuracy and A_{sat} .

mance is caused by the limitation of the dimension. Figure 11 shows that the peak timing error of KFMT with the highest probability density has much less offset from the zero timing error than that of DLKF. This means that KFMT can improve the performance. In fact, its synchronization accuracy achieves 0.275 nsec which is smaller than the aimed accuracy of 0.3 nsec.

Next, we investigate the relationship between A_{sat} and synchronization accuracy on the condition of $\sigma_v = 0.5$ nsec. We change the amplitude of $s_{sat}(t)$ and plot the timing error of synchronization for each synchronization method in Fig. 12. The accuracy of DLKF significantly varies with A_{sat} . When $s_{sat}(t)$ can be neglected, the accuracy of DLKF is approximately equal to that of KFMT. However, the accuracy of DLKF becomes considerably worse with increase of A_{sat} . For $A_{sat} > 500$ nsec, the synchronization error for DLKF is worse even than the fixed filter. KFMT has much better performance than that of DLKF especially for large A_{sat} .

5. Conclusions

In this paper, we have investigated synchronization methods for synchronous CDMA broadband communication systems with a GEO satellite. High bit-rate synchronous CDMA systems require extremely accurate synchronization which is not satisfied by conventional fixed filters. The synchronization method using Kalman filter is an attractive candidate for this purpose. However, satellite motion effect $s_{sat}(t)$ requires a large dimensional system for Kalman filter, which is not realistic to implement practical systems because transmitting timings should be determined in real time. In order to overcome the defect of the conventional Kalman filter, we have proposed a synchronization method KFMT based on the approximation which assume that $s_{sat}(t)$ can be dealt with as a linear function. The synchronization method KFMT has dealt with $s_{sat}(t)$ and other signals separately. It was clarified that the proposed synchronization method can achieve synchronization accuracy of 0.275 nsec, which means that Gigachip rate synchronous CDMA systems are feasible.

Acknowledgment

We thank Prof. Toru Sato of Kyoto University, for his valuable advice and encouragement. This work is supported in part by the 21st Century COE Program (Grant No. 14213201).

References

- [1] R. de Gaudenzi, C. Elia, and R. Viola, "Bandlimited quasi-synchronous CDMA," IEEE J. Sel. Areas Commun., vol.10, no.2, pp.328–343, Feb. 1992.
- [2] W.R. Braun, D. Dzung, P. Eglin, G. Mastner, and P. Rauber, Definition of the Mobile Network Synchronization Experiment, ESA Contract no.8728/90/NL/RE Asea Brown Boveri Corporate Research, Jan. 1991.
- [3] C. Soprano, "A feedback control loop for autonomous time synchronisation for mobile satellite systems, including satellites in any earth orbit," ESA Journal, vol.17, pp.57–71, 1993.
- [4] C. Soprano, "A CDMA synchronisation scheme," Proc. IMSC JPL PUBL, pp.437–442, 1993.
- [5] T. Sakamoto, D. Umehara, and M. Kawai, "A synchronization method for synchronous CDMA systems with GEO satellites," IEICE Technical Report, SAT2001-69, Oct. 2001.
- [6] NASDA NEWS, no.256, pp.1–2, March 2003.
- [7] Sophia Wireless Inc., "Ka-band solid-state amplifiers at TWTA power levels," Microwaves Journal, pp.162–164, Feb. 2004.
- [8] M. Kawai, T. Sato, D. Umehara, I. Kimura, Y. Yamauchi, J. Terazono, and T. Baba, "Ka-band satellite communication link performance exploiting a small earth station," Proc. Commun. Conf. IEICE 2001, B-3-1, p.202, Sept. 2001.
- [9] E. Vilar and S. Senin, "Propagation phase noise identified using 40 GHz satellite downlink," Electron. Lett., vol.33, no.22, pp.1901–1902, Oct. 1997.
- [10] E. Vilar and H. Smith, "A theoretical and experimental study of angular scintillations in earth space paths," IEEE Trans. Antennas Propag., vol.AP-34, no.1, pp.2–10, Jan. 1986.
- [11] G.M.R. Winkler, "Path delay, its variations, and some implications for the field use of precise frequency standards," Proc. IEEE, vol.60, no.5, pp.522–529, May 1972.
- [12] J.J. Spilker, Jr., "Delay-lock tracking of binary signals," IEEE Trans. Space. Electron. Telemetry, vol.SET-9, no.3, pp.1–8, March 1963.
- [13] R.E. Kalman and R.S. Bucy, "New results in linear filtering and prediction theory," Trans. ASME, vol.83D, no.1, pp.95–108, 1961.
- [14] H. Akaike, "Information theory and an extension of the maximum likelihood principle," 2nd International symposium on Information theory, ed. B.N. Petrov and F. Csaki, pp.267–281, 1973.
- [15] D.W. Marquardt, "An algorithm for least-squares estimation of non-linear parameters," J. Soc. Indust. Appl. Math., vol.11, no.2, pp.431–441, 1963.
- [16] J.E. Prussing and B.A. Conway, Orbital Mechanics, chap. 8, Oxford Univ. Press, 1993.

Appendix: Satellite Motion Effect

Satellite motion effect $s_{sat}(t)$ is given as

$$s_{sat}(t) = s_{FES}(t) - s_{NCS}(t), \quad (\text{A} \cdot 1)$$

where $s_{FES}(t)$ and $s_{NCS}(t)$ are the time variation of satellite motion for FES and NCS, respectively. Investigating the amplitude of $s_{sat}(t)$ is an important issue.

$s_{FES}(t)$ is expressed as

Table A-1 Amplitude of satellite motion effect for the most eastern, western, southern and northern places in Japan.

Place	Location	Amplitude
Cape Nosappu (the most eastern)	(146,43)	2053 nsec
Yonaguni Island (the most western)	(123,24)	3485 nsec
Hateruma Island (the most southern)	(124,24)	3618 nsec
Cape Souya (the most northern)	(142,46)	2579 nsec

$$s_{\text{FES}}(t) = A_{\text{sat}} \sin(\omega t + \phi), \quad (\text{A}\cdot 2)$$

$$= A_1 \cos(\omega t + \alpha_1) + A_2 \cos(\omega t + \alpha_2), \quad (\text{A}\cdot 3)$$

where $\omega = 2\pi/(24 \times 60 \times 60)$ rad/sec, and α_1 and α_2 depend on the schedule of station keeping [16]. A_1 and A_2 are determined as

$$A_1 = ae \sqrt{u^2 + 4v^2}, \quad (\text{A}\cdot 4)$$

$$A_2 = ai|w|, \quad (\text{A}\cdot 5)$$

where $a = 42164$ km is the orbital radius, e is an eccentricity, and i is an inclination. u, v, w are called sensitivity coefficients expressed as

$$u \equiv \cos \phi \cos \theta, \quad (\text{A}\cdot 6)$$

$$v \equiv -\cos \phi \sin \theta, \quad (\text{A}\cdot 7)$$

$$w \equiv -\sin \phi, \quad (\text{A}\cdot 8)$$

where θ and ϕ are defined as

$$\theta = \tan^{-1} \frac{r \cos \psi \sin \lambda}{a - r \cos \psi \cos \lambda}, \quad (\text{A}\cdot 9)$$

$$\phi = \tan^{-1} \frac{r \sin \psi}{\sqrt{a^2 - 2ar \cos \psi \cos \lambda + r^2 \cos^2 \psi}}, \quad (\text{A}\cdot 10)$$

where we define $\lambda = \lambda_F - \lambda_S$. The FES is located in ψ degrees of north latitude, λ_F degrees of east longitude, the satellite is located at λ_S degrees of east longitude, and the radius of the earth is $r = 6378$ km. To evaluate the synchronization accuracy in the worst case, we assume $\alpha_1 = \alpha_2$ which means the two sinusoids have the same phase in $s_{\text{sat}}(t)$. We search the maximum amplitude of $s_{\text{sat}}(t)$ among the places in Japan where people live.

The satellite motion effect for the NCS $s_{\text{NCS}}(t)$ can be calculated in the same way. Table A-1 shows $|s_{\text{sat}}(t)|$ for the most eastern, western, southern and northern points in Japan. We see the maximum value of $|s_{\text{sat}}(t)|$ is 3618 nsec at Hateruma Island in Japan.



Takuya Sakamoto received the B.E. degree from Kyoto University in 2000, the M.I. degree from Graduate School of Informatics, Kyoto University in 2002. He is currently studying for the Ph.D. degree at Graduate School of Informatics, Kyoto University. His current research interest is in digital signal processing. He is a member of the IEEE and the IEEEJ.



Daisuke Umehara received the B.S. degree from Nagoya University in 1994, the M.I. degree from Japan Advanced Institute of Science and Technology in 1996, the D.E. degree from Tokyo Institute of Technology in 1999. He is currently a research associate at Graduate School of Informatics, Kyoto University. He has been engaged in research work on digital communication systems, coding theory, and digital signal processing. Dr. Umehara is a member of the IEEE.



Yoshiteru Morihoro received the B.S., M.S. and Ph.D. degrees from Tokyo Institute of Technology in 1967, 1970 and 1973, respectively. During 1973–1998 he worked mainly for research and development of satellite communication systems at Nippon Telegraph and Telephone Corporation (NTT). Since 1998 he is a Professor in the Graduate School of Informatics, Kyoto University. He was a recipient of the IEICE Young Investigators Award in 1976 and the IEICE Achievement Award in 1992. He was engaged to be a general chair of the 7th International Symposium on Power-Line Communications and Its Applications (ISPLC2003).



Makoto Kawai received his B.S., M.S. and Dr. Eng. degrees in electrical engineering from Kyoto University, Kyoto, Japan, in 1972, 1974 and 1987, respectively. Since 1974, he worked mainly for research and development of wireless communication systems at Nippon Telegraph and Telephone Corporation (NTT). He was an associate professor at Graduate School of Informatics, Kyoto University from 1999 to 2003. He is now a professor of Faculty of Science and Engineering, Ritsumeikan University, Shiga, Japan.